Article

Chemical Reactivity of Aloe-Emodin and Its Hydroxylation Metabolites to Thiols

Xu Wang, Xin Xin, Ying Sun, Lizhu Zou, Hui Li, Yufei Zhao, Ruihong Li, Ying Peng, and Jiang Zheng

Chem. Res. Toxicol., **Just Accepted Manuscript** • DOI: 10.1021/acs.chemrestox.8b00248 • Publication Date (Web): 23 Jan 2019

Chemical Reactivity of Aloe-Emodin and Its Hydroxylation Metabolites to Thiols

Xu Wang,[¶,†] Xin Xin,[¶,†] Ying Sun,[†] Lizhu Zou,[†] Hui Li,[†] Yufei Zhao,[†] Ruihong Li,[†] Ying Peng,*[,†] and Jiang Zheng*[,†,§]

[†]Wuya College of Innovation, Shenyang Pharmaceutical University, Shenyang, Liaoning, 110016, P.R. China

[§]State Key Laboratory of Functions and Applications of Medicinal Plants, Key Laboratory of Pharmaceutics of Guizhou Province, Guizhou Medical University, Guiyang, Guizhou, 550025, P.R. China

***Corresponding Authors:**

Jiang Zheng, PhD

Wuya College of Innovation, Shenyang Pharmaceutical University, No. 103, Wenhua Road, Shenyang, Liaoning, 110016, P. R. China

State Key Laboratory of Functions and Applications of Medicinal Plants, Key Laboratory of Pharmaceutics of Guizhou Province, Guizhou Medical University, 9 Beijing Road, Guiyang, Guizhou, 550025, P.R. China

Email: zhengneu@yahoo.com

Tel: +86-24-23986361; Fax: +86-24-23986510

Ying Peng, PhD

Wuya College of Innovation, Shenyang Pharmaceutical University, No. 103, Wenhua Road, Shenyang, Liaoning, 110016, P. R. China

Email: yingpeng1999@163.com

Tel: +86-24-23986361; Fax: +86-24-23986510

¶: The two authors contributed equally to this work.

†, §: The two corresponding units contributed equally to this work.

TOC Graphic

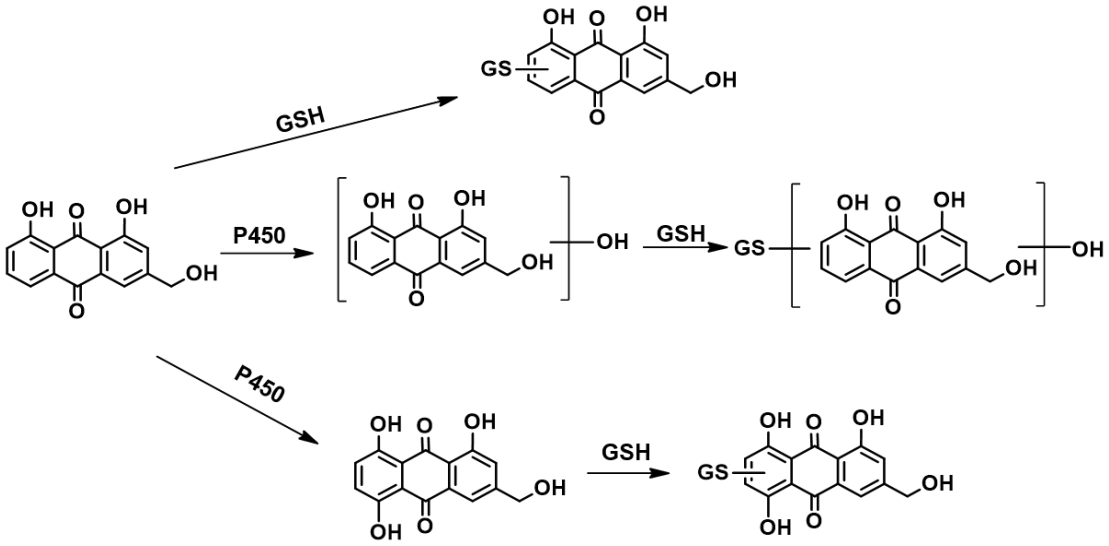

ABSTRACT

Aloe-emodin (AE), an anthraquinone derivative, is a bioactive ingredient isolated from Rhubarb which is used to treat inflammatory illnesses in China and many other countries in Asia. AE has shown a wide range of pharmacological effects. Recent studies showed that exposure to AE could cause DNA damage and cytotoxicity. The goals of the present study aimed at 1) exploration of oxidative metabolism pathways of AE, 2) identification of P450 enzymes which respond the hydroxylation of AE, and 3) determination of electrophilicity of AE and its oxidative metabolites. Two hydroxylation metabolites (M1 and M2) and four GSH conjugates (M3-M6) were found in incubations consisting of AE, rat or human liver microsomes, and NADPH supplemented with GSH. Conjugates M3 and M4 came from AE itself, and M5 and M6 originated from M1 and M2 individually. M1 and M2 (5-hydroxy aloe-emodin) and M3-M6 were also detected in rat primary hepatocytes after exposure to AE. Additionally, biliary M3, M4 and M6 were detected in rats given AE. Urinary M1, M2 and M7 (a NAC conjugate) were observed in animals administered AE. Recombinant P450 enzyme incubations illustrated that hydroxylation of AE was primarily catalyzed by P450 1A2, 3A4 and 3A5. The metabolism investigation will help us to better understand the biochemical mechanisms of cytotoxicity induced by AE.

INTRODUCTION

Rhubarb (*Rheum rhabarbarum*), a famous herb known as traditional Chinese medicine, is widely utilized for the treatment of many diseases, such as constipation, jaundice, and gastrointestinal bleeding and ulcers.[1] Rhubarb is often employed in many Chinese herbal medicine formulations applied for the treatment of inflammation, including acute cholecystitis, rheumatoid arthritis and acute appendicitis.[2] Rhubarb also reportedly showed anti-bacterial, antioxidant, anti-cancer, anti-angiogenesis and anti-inflammation properties.[3-6] Aloe-emodin (AE) is one of major natural anthraquinone ingredients in Rhubarb.[7] Recently, AE has caught much attention because of its various pharmacologic properties, including cardiovascular protection, laxative, antifungal, antiviral, skin conditioning, and immune regulation effects.[8] According to recent reports, AE revealed selective inhibitory effect on the growth of neuroectodermal tumors.[9] Meanwhile, AE was reported to strengthen anticancer effect when co-administered with cisplatin, doxorubicin, docetaxel, and 5-fluorouracil.[10] In addition, AE enhanced chemotherapeutic efficacy of anticancer agents (doxorubicin, *cis*-platinol, 5-fluorouracil, and the tyrosine kinase inhibitor STI 571) in Merkel skin carcinoma cells,[11] suppressed the growth of NCI-H460 (human lung cancer cells)[12] and the proliferation of MKN45 gastric cancer cells.[10]

Interference of DNA functioning, such as DNA damage, is one of the most common mechanisms of antitumor action. Camptothecin is a topoisomerase I (Top1) inducer, which induces Top1-mediated DNA damage resulting in reduced cell proliferation and survival.[13,14] Similarly, anthraquinone anticancer drugs

demonstrated cytotoxic activities through their interaction with guanine/cytosine rich sites of DNA preferentially.[15] The suppression of DNA replication is thought to result from certain conformational changes in the DNA.[16] Furthermore, anthroquinones were reported to produce topoisomerase II-mediated DNA damage.[15] AE was found to induce primary DNA damage in the liver and even in the kidney, which indicates a genotoxic mechanism of action involved *in vivo*.[17] In addition, micronucleus assay displayed genotoxicity induced by AE itself and its metabolites in Salmonella typhimurium strains TA98 and TA1537.[17] A recent study showed that exposure to AE and UV light (320-400 nm) induced phototoxicity in cultured human skin fibroblast cells.[18] Moreover, Strickland et al. reported the enhancement UV light-induced malignant melanoma in C3H mice after topical treatment of AE.[19]

In this study, we defined the oxidative metabolism pathways of AE in liver microsomal incubations, cultured primary rat hepatocytes and rats, identified the P450 primary enzymes which participated in the oxidation of AE, and determined the chemical reactivity of AE and its hydroxylation metabolites towards biological thiols.

EXPERIMENTAL PROCEDURES

Chemicals and Materials.

AE (≥ 98%) was provided by Chengdu Pufeide Biologic Technology Co., Ltd (Chengdu, China). Human liver microsomes and recombinant human P450 enzymes were acquired from BD Gentest (Woburn, MA). Rat (Sprague-Dawley, male) liver microsomes were pre-prepared in our laboratory in accordance with previous literature.[20] Distilled water and organic solvent were obtained from Wahaha Co., Ltd. (Hangzhou, China) and Fisher Scientific (Springfield, NJ), respectively. Glutathione (GSH), *S*-hexylglutathione, *N*-acetylcysteine (NAC), and reduced nicotinamide adenine dinucleotide phosphate (NADPH) were purchased from Sigma-Aldrich (St. Louis, MO).

Microsomal Incubation.

AE (27 mg) was dissolved in 10 mL dimethyl sulfoxide (DMSO) to offer the stock solution. Test compound AE (100 μM) was mixed with rat or human liver microsomes (1.0 mg protein/mL) in PBS buffer (pH 7.4) and $MgCl_2$ (3.2 mM) fortified with GSH (10 mM) (final volume: 250 μL, final organic solvent content: 0.5%). The microsomal solution was further mixed with NADPH (1.0 mM) to initiate the reactions. Control groups excluded NADPH. Incubation of the resulting mixtures was carried out in a water bath shaker. After incubation at 37 °C for 45 min, the reactions were terminated by addition of the same volume of cold CH_3CN (-20 °C). Deproteinization was achieved by 10 min centrifugation at 19,000g at 4 °C, and the supernatants were analyzed by LC-MS/MS. Each

incubation was repeated twice. Similar microsomal incubations were carried out except the absence of GSH.

Cell Experiments.

All animal operation procedures were authorized by the Ethics Review Committee for Animal Experimentation of Shenyang Pharmaceutical University (license number: SYPU-IACUC-C2018-6-8-201). Male Sprague-Dawley rats (200±20 g) were obtained from the Animal Center of Shenyang Pharmaceutical University. Rats were kept on standard rat chow at room temperature and moderate humidity with 12 h dark/light cycles. Animals were starved for 12 h and were anesthetized by use of 10% chloral hydrate (35 mg/kg). Subsequently, rats (except the head) were soaked in 75% ethanol for 10 s. The rats were fixed, and the abdomen was opened to expose and isolate the portal vein. An intravenous syringe (detaining needle) was inserted into the portal vein. The liver was perfused with perfusion fluid containing 1,000 U/mL heparin. At the same time, the inferior vena cava was cut in order to discharge the perfusate. When the color of the liver was changed from light red to pale yellow, the liver was separated and transferred to sterile petri dishes. The liver was perfused with 0.05% calcium-containing collagenase IV perfusate at 37 °C at the speed of 5 mL/min until the liver became soft and fragile. The liver was transferred to a pre-cooled medium containing DMEM. The hepatocyte suspensions were filtered through a 100 mesh filter to get rid of connective tissues and then centrifuged at 300 rpm (3 min) and 4 °C. The supernatants were discarded, and the resulting cell pellets were suspended in a density

separation solution, followed by 5 min centrifugation at 500 rpm and 4 °C.[21] The supernatants were discarded, and the resulting hepatocyte pellets were placed in culture media containing 20% FBS. The number and viability of cells were measured by trypan blue exclusion. Only cells with a viability > 80% were used for metabolism tests. Cells were incubated in media containing insulin (0.5 mg/L), dexamethasone (1.0 μM) and double antibody (1%). The cell density was 1×10^5/mL. All operations were carried out under aseptic conditions.

Cells were incubated with AE and vehicle DMSO for 12 h under 5% CO_2 at 37 °C in an incubator. The resultant cell suspension was mixed with three volumes of cold CH_3CN (-20 °C) for deproteinization. The resulting supernatants (10 μL) were analyzed by an LC-MS/MS system.

Chemical Synthesis of AE Metabolites.

Chemical synthesis of M1 and M2 were performed in accordance with a published protocol.[22] In short, potassium persulfate (208 mg) was slowly added into a sulfuric acid solution (4 mL) containing AE (80 mg) with stirring. The resulting solution was further stirred for another 15 min at room temperature, followed by mixing with an excess of potassium persulfate (208 mg), stirring at 50 °C for 1 h, and mixing with 80 mL water and sodium metabisulfite (800 mg). The resultant suspension was extracted with butanol (3×4 mL). The butanol extracts were pooled, washed with dilute hydrochloric acid (3×12 mL) and water (3×12 mL), dried with anhydrous Na_2SO_4, and concentrated by vacuum evaporation. A semi preparative HPLC system was employed for product purification. The purified products were

characterized by MS and NMR. All NMR spectra were acquired on a BRUKER-ARX-600 spectrometer (600 MHz).

Synthesis of GSH conjugates M3 and M4 was achieved by mixing of AE (0.05 μmol) with GSH (10 μmol) in PBS buffer (0.5 mL, pH 7.4), and the resulting solution was stirred for 1 h at 37 °C and centrifuged at 19,000 *g* for 10 min. The resultant supernatants were subjected to the LC-MS/MS system for analysis.

Synthetic GSH conjugates M5 and M6 were prepared as following: M1 (3.48 μmol) and M2 (3.48 μmol) were separately dissolved in 1.0 mL of methanol, and then mixed with GSH (20 mM) in 10 mL PBS buffer (pH 7.4). After stirring at 40 °C for 1 h, the resulting mixture was centrifuged at 19,000 *g* for 10 min and analyzed by an LC-MS/MS system.

Animal Experiments

Male Sprague−Dawley rats (200±20 g) were purchased from the Animal Center of Shenyang Pharmaceutical University were kept on standard rat chow at room temperature and moderate humidity with 12 h dark/light cycles. Animals were randomly split into two groups, and each group contained 3 rats. The animals were starved for 24 h before any treatment. Rats of group one were administered chloral hydrate (10%, 3.0 mL/kg, i.p.), and bile ducts of the anaesthetized rats were cannulated, followed by collection of blank bile. Subsequently, the cannulated rats were intraperitoneally given corn oil solution of AE (200 mg/kg), and then 0–12 h bile samples were harvested. Rats of the other group were treated with the same dose of AE (i.p.) and kept in metabolism cages individually. The rats were

permitted to reach food and water during the experiment, and 0-24 h urine samples were collected, along with blank urine samples before the administration of AE.

Recombinant Human P450 Incubations.

Similar procedure was followed for recombinant P450 incubations as for that of microsomal reactions described above. The individual human P450 enzymes (100 nM) included P450s 1A2, 2A6, 2B6, 2C9, 2C19, 2D6, 2E1, 3A4, and 3A5. The final reaction volume was 250 μL. The resulting enzymatic reactions were terminated by mixing with 250 μL cold CH_3CN (-20°C) containing *S*-hexylglutathione (the internal standard, 50 ng/mL), followed by 30 s vortex mixing and 10 min centrifuging at 19,000 *g*. The resultant supernatants were submitted to an LC-MS/MS system for analysis as below. The generation of the corresponding products was monitored and regarded as individual enzyme activity. Normalization of reaction rates for individual P450 enzymes (NRR) was achieved by the following equation.[23]

$$NRR = RMP \times MSC$$

Where RMP: the rates of metabolite production in incubations with the individual recombinant P450 enzymes; MSC: the mean specific content of the corresponding P450 enzyme in human liver microsomes.

Sample Preparation for LC-MS/MS Analysis

Cleaning of bile and urine samples was achieved on C18 SPE cartridges. Bile and urine samples (pH=3-4, 200 μL) were individually loaded onto SPE cartridges

which had been washed with methanol and then diluted acetic acid (pH 3-4). The resulting cartridges were washed with deionized water (pH 3-4, acidified with acetic acid), followed by eluting with a series of gradient methanol solutions (10, 20, 30, 40, 50, 60, 70, 80 and 90%). The resulting eluates were concentrated by blowing with nitrogen gas, and the residues were dissolved with 10% CH_3CN in water (200 μL). After 10 min centrifuging at 16,000 *g* and 4 °C, and the resulting supernatants (10 μL) were submitted to the LC-MS/MS for analysis.

LC-MS/MS Method.

All separations and analyses of samples were conducted on an LC-MS/MS composed of a 1260 infinity LC system (Agilent Technologies, Biblingen, Germany) and an inline AB SCIEX Instruments 5500 triple quadrupole mass spectrometer (Applied Biosystems, Foster City, CA, USA). An Accuore C18 column (4.6×150 mm, 5μm; Thermo Fisher, Inc., Pittsburgh, PA) was employed for analyte separation with flow rate of 0.8 mL/min and column temperature of 25 °C. Solvent A was CH_3CN with 0.1% formic acid and solvent B was water with 0.1% formic acid. The gradient elution program was set as follows, 0-2 min: 10% solvent A, 2-10 min: 10%-95% A, 10-15 min: 95% A, 15-16 min: 90%-10% A, 16-18 min: 10% solvent A. The parameters of mass spectrometric analyses were set after optimization as follows, gas 1: 50 psi, gas 2: 50 psi, curtain gas: 35 psi, ion source temperature (TEM): 650 °C, ion spray voltage (IS): 5,500, declustering potential (DP): 110 V, entrance potential (EP): 10 V, collision cell exit potential (CXP): 13 V. Detection of AE, hydroxylation metabolites of AE, GSH conjugates, and NAC conjugate was achieve

by monitoring precursor/product ion pairs (collision energy, CE) *m/z* 271→225 (35), *m/z* 287 →241 (35), *m/z* 576 →301 (42)/592 →317 (42), and 448 →317 (40), respectively. Analysis of *S*-hexylglutathione was performed by scanning ion pair (DP, CE) *m/z* 392→246 (86, 24).

Additionally, an AB SCIEX Instruments 4000 Q-Trap mass spectrometry equipped with a 1260 infinity LC system was used for enhanced product ion (EPI) analysis which allowed us to accumulate mass spectral information for all metabolites/products interested. The information-dependent acquisition (IDA) was utilized to launch EPI spectrum when ions acquired via multiple reaction monitoring (MRM) reached over 1,000 cps. The collision energy (CE) was 40 eV with an extendibility of 15 eV. Positive mode was employed for EPI acquisition by scanning product ions at a range of *m/z* 50 to 600. AB SCIEX Analyst 1.6.2 software was employed to process mass spectrometric data.

Analysis of synthetic metabolites was also carried out on a hybrid quadrupole-time-of-flight (Q-TOF) mass system (micro Q-TOF, Bruker Corporation, Billerica, MA) equipped with an inline Agilent 1200 Series Rapid Resolution LC system. Analysis was performed in positive-ion mode. Mass spectrometric parameters were optimized as follows. Capillary voltage: -4,500 V, end plate offset: 2,500 V, nebulizer gas pressure: 1.2 bar, temperature: 180 °C, the dry gas flow rate: 8.0 L/min. The spectra were obtained at 2 s per spectrum ranging *m/z* 50 to 1,500. Similar LC parameters were applied for analyte separation as described above. Bruker Daltonics Data Analysis 3.4 software was employed to process mass

spectrometric data.

RESULTS

Mass Spectrometric Property of AE.

Mass spectral behavior of AE was determined to gain major fragments of the parent compound. Ionization in positive mode was found to provide more fragment ions and much higher sensitivity than that in negative ionization mode. As shown in Figure 1, AE displayed *m/z* 115 ($[M+H-H_2O-4CO-C_2H_2]^+$), 141 ($[M+H-H_2O-4CO]^+$), 169 ($[M+H-H_2O-3CO]^+$), 197 ($[M+H-H_2O-2CO]^+$), and 225 ($[M+H-H_2O-CO]^+$) of fragment ions with molecular ion of *m/z* 271.

Formation of Oxidative Metabolites

Liver microsomal incubations (both rat and human) of AE produced two oxidative metabolites (M1 and M2) with their retention time at 9.53 and 12.0 min (Figure 2B). NADPH was required for the production of the two oxidative metabolites (Figure 2A). This suggests the involvement of P450 enzymes in the generation of M1 and M2.

The observed $[M]^+$ of M1 and M2 allowed us to consider that the formation of the metabolites resulted from hydroxylation, and that they are positional isomers arising from the location of hydroxyl group. The tandem mass spectra of M1 and M2 displayed product ions *m/z* 139 ($[M+H-2H_2O-4CO]^+$), 157 ($[M+H-H_2O-4CO]^+$), 185 ($[M+H-H_2O-3CO]^+$), 213 ($[M+H-H_2O-2CO]^+$), and 241 ($[M+H-H_2O-CO]^+$) obtained from MRM-EPI scanning (*m/z* 287/241) (Figure 2E, F). The fragment ions at *m/z* 157, 185, 241 and 257 of M1 and M2 were 16 Da higher than ions *m/z* 141, 169, 225 and 241 of AE (Figure 1), which suggests that M1 and M2 were the products of

metabolic hydroxylation of AE. Traces of M1 and M2 were found in the authentic sample, and the observed the contaminated M1 and M2 may result from auto-oxidation.

Chemical synthesis of M1 and M2 was achieved by oxidation AE with potassium persulfate in H_2SO_4. The resulting products displayed identical retention time and mass spectral behaviors as M1 and M2 generated in microsomal reactions (Figure 2C, D, G, and H). High resolution mass spectrometry analysis of synthetic M1 revealed its protonated molecular ion of *m*/*z* 287.0550, consistent with the corresponding theoretical mass within 5 ppm compared with the predicted formula (Table 1). Unfortunately, we were not able to gain satisfactory NMR spectrum of M1. Synthetic M2 was purified and analyzed by NMR for characterization. ^{1}H NMR ($CDCl_3$, 600 MHz): δ 4.85 (2H, S, H-11), 7.31 (1H, d, *J*=9.4 Hz, H-7), 7.33 (1H, d, *J*=9.4 Hz, H-6), 7.37 (1H, br. s, H-2), 7.87 (1H, br. s, H-4), 12.22 (1H, s, 1-OH), 12.32 (1H, s, 8-OH), 13.02 (1H, s, 5-OH). M2 was assigned to be 5-hydroxy aloe-emodin.

Formation of GSH Conjugates.

Four GSH conjugates (M3-M6) were detected in AE-fortified human or rat liver microsomes supplemented with GSH (Figures S2 and 3). M3 and M4 with identical molecular ion of *m*/*z* 576 eluted at 7.95 and 8.30 min (Figure 3B). In addition, the mass spectra demonstrated characteristic product ions related to the cleavage of GSH portion (Figure 3D, E). Primary product ion *m*/*z* 301 arose from the segmentation of the C-S of the GSH portion (−273 Da) and the loss of two

hydrogen atoms from the GSH conjugates (*m*/*z* 576). Fragment ions *m*/*z* 501 and 430 resulted from the GSH conjugates (*m*/*z* 576) after losing the glycinyl portion (−75 Da) and glutaminyl portion (−146 Da). Product ion *m*/*z* 327 came from the loss of the *N*-formylglycinyl section (−103 Da) from *m*/*z* 430. Meanwhile, both M3 and M4 were found in NADPH-absent microsomal incubations (Figure 3A). Mixing and reaction of GSH and AE in buffer offered two GSH conjugates whose chromatographic and mass spectrometric identities (Figure 3C, F and G) are consistent with those of M3 and M4 formed in microsomal incubations. However, owing to poor yields of the reactions, we failed to gain sufficient quantities of the two compounds to be characterized by NMR.

The formation of M5 and M6 (retention time = 7.73 and 8.16 min) was monitored by acquiring precursor/product ion pair *m*/*z* 592→317 (Figure 4B). The observed molecular ions of *m*/*z* 592 corresponded to the molecular weight of the conjugates composed of a molecule of GSH and a molecule of hydroxylation metabolites of AE, and the mass spectra revealed the indicative characteristic product ions related to the loss of GSH portion (Figures 4D and 5D). Primary fragment ion *m*/*z* 317 is a result that *m*/*z* 592 lost the GSH portion but without the loss of the sulfur atom (−273 Da). The cleavage of the glycinyl portion (−75 Da) and glutaminyl section (−146 Da) from *m*/*z* 592 resulted in the formation of fragment ions *m*/*z* 517 and 446, respectively. Ion *m*/*z* 343 consequently came from the deprivation of the *N*-formylglycinyl group (103 Da) derived from product ion *m*/*z* 446. The observed fragment ion *m*/*z* 463 was a result of the neutral loss (NL) of the *γ*-glutamyl portion

(129 Da) from fragment *m*/*z* 592. A trace amount of M6 was observed in microsomal reaction without incorporation of NADPH (Figure 5A), perhaps resulting from the product of AE auto-oxidation. Additionally, the $[M+H]^+$ of M5 and M6 (*m*/*z* 592) was 16 Da more than that of M3 and M4, and the product ions of M3 (*m*/*z* 301) and M4 (*m*/*z* 501) were both 16 Da less than that of M5 (*m*/*z* 317) and M6 (*m*/*z* 517), respectively. This suggests that M5 and M6 were generated from the conjugation of hydroxylation metabolites of AE with a molecule of GSH.

To identify the metabolic pathways of M5 and M6 (GSH conjugates), synthetic M1 and M2 were directly and individually mixed and stirred with GSH. The product in the M1-GSH mixture displayed identical chromatographic behavior and fragment pattern as that of M5 observed in microsomal reactions (Figure 4C and E). On the other hand, the product obtained in the M2-GSH mixture and M6 also revealed identical retention time and mass spectrometric identities (Figure 5C and E). This allows us to propose that M5 and M6 resulted from the conjugation of a molecule of GSH with M1 and M2, respectively. Unfortunately, we failed to obtain pure M5 and M6 for NMR characterization, since the two GSH conjugates were decomposed during the process of purification.

Formation of Oxidative Metabolites in Primary Hepatocytes.

To investigate the metabolism of AE in hepatocytes, oxidative metabolites generated in cultured primary rat hepatocytes were characterized using LC–MS/MS. Two oxidative metabolites were found in primary hepatocytes exposed to AE (Figure 6B). As expected, such metabolites were not found in primary hepatocytes treated

with vehicle (Figure 6A). Similar observation in retention time and fragment patterns of the oxidative metabolites in hepatocytes was obtained with those of M1 and M2 generated in both chemical synthesis and microsomal reactions (Figures 2E, F and 6C, D).

Four metabolites (tentatively M3/M4 and M5/M6) displaying their $[M+H]^+$ at *m*/*z* 576 and 592 were observed in cultured rat hepatocytes after exposure to AE (Figures 7B and 8B). The four metabolites are considered to be GSH conjugates originating from AE and hydroxylated AE, respectively, based on the $[M+H]^+$ of *m/z* 576 and 592 observed. In addition, the metabolites found in the cells demonstrated the same chromatographic identity and fragment patterns as those of M3/M4 and M5/M6 observed in microsomal reactions (Figures 7C, D and 8C, D). As expected, none of the GSH conjugates was observed in hepatocytes treated with vehicle (Figures 7A and 8A).

Biliary and Urinary Metabolites of AE

In vivo AE metabolism study was carried out in rats. Bile and urine samples were collected, followed by LC-MS/MS analysis. No AE-derived GSH conjugates were observed in blank bile samples (Figure 9A, B), while three GSH conjugates (M3, M4 and M6) with $[M+H]^+$ at *m*/*z* 576 and 327 (M3 and M4), *m*/*z* 592 and 317 (M6) were found in the bile of the animals treated with AE (Figure 9C, D). The metabolites observed *in vivo* study (Figure 9C, D, E, F and G) were consistent with those found in microsomal incubations (Figures 3B, D, E, and 5B, D) in aspects of chromatographic and mass spectrometric behaviors. However, we failed to find M5

(a hydroxylated AE GSH conjugate) from the bile of rats treated with AE.

Hydroxylation metabolites M1 and M2 were observed in urine samples obtained from rats after an intraperitoneal injection of AE (Figure 10B, C), and neither of the two metabolites was found in blank urine (Figure 10A). The urinary metabolites demonstrated similarity in their retention time and major fragmentation patterns (Figure 10B, C, D and E) as that of the corresponding metabolites produced in microsomal reactions (Figure 2B, E and F). Nevertheless, the analysis of urine samples from AE treated rats showed no AE-derived GSH conjugates. Instead, a new metabolite (M7) was detected with $[M+H]^+$ at *m*/*z* 448 in agreement with the molecular weight of the corresponding NAC conjugate, i.e. the conjugate composed of a molecule of hydroxylation metabolite of AE and a molecule of NAC (Figure 11B). Again, the conjugate was not found in urine of rats given vehicle (Figure 11A).

As shown in Figure 11B, urinary M7 eluted at 9.63 min and was detected by scanning precursor/product ion pairs *m*/*z* 448 and 317 in positive ion mode. Primary fragment ion *m*/*z* 317 was derived from the loss of NAC without sulfur from *m*/*z* 448. Fragment ion *m*/*z* 343 was generated from the loss of acetylamino and carboxylic acid portions (105 Da) from *m*/*z* 448. Product ion *m*/*z* 130 originated from NAC moiety absent of sulfur. Product ion *m*/*z* 319 resulted from the neutral loss of the glutamyl moiety (−129 Da) from *m*/*z* 448. This suggests that M7 was the conjugate composed of a molecule of NAC and a molecule of oxidative metabolite of AE. As expected, an NAC conjugate was observed in an AE- and NADPH-fortified rat microsomal

incubations trapped with NAC. The NAC conjugate was found to share the identical chromatographic and mass spectrometric properties with the urinary NAC conjugate, as shown in Figure 11C, E and D.

P450 Enzymes Participating in AE Metabolism.

Characterization of P450 enzymes participating in metabolic AE hydroxylation was achieved by monitoring the production of M1, M2, M5 and M6 in incubation of AE with individual recombinant human P450 enzymes fortified with NADPH and GSH. P450s 1A2, 3A4, and 3A5 displayed the catalytic property in the production of M1, M2 and M5. Additionally, P450 1A2 was found to show the most effectiveness for the catalytic hydroxylation among the three (Figure 12A, B). However, the generation of M6 can apparently be "catalyzed" by all P450 enzymes tested. We found that M6 was derived from M2 some of which possibly came from auto-oxidation of AE. In other word, partial M6 might result from the spontaneous reaction of GSH with contaminated M2.

DISCUSSION

We attempted to study *in vitro* biotransformation of AE to better understand the biochemical mechanism of AE cytotoxicity. Initially, the fragmentation pattern of parent compound AE were explored (Figure 1), which assists us to characterize the structure of AE metabolites.

Two hydroxylation metabolites (M1 and M2) were observed in incubation mixture containing AE and rat or human liver microsomes. The amount of M1 produced in human liver microsomal (HLM) incubation system was about three times higher than that in the rat liver microsomal (RLM) system. The amount of M2 produced in HLMs was about two times higher than that produced in RLMs (Figures S1-3). Apparently, human liver microsomes showed higher activity then rat liver microsomes to catalyze the hydroxylation of AE. NADPH was required for the formation of the two oxidative metabolites. As shown in Scheme 1, the oxidative metabolism and GSH conjugation pathways of AE is proposed from the obtained mass spectrometric data. M1 and M2 were chemically synthesized to verify the structures of the oxidative metabolites. M2 was assigned as 5-hydroxy aloe-emodin based on its NMR data (Figure S4). Unfortunately, we failed to gain a quality of NMR spectrum of M1 for structural identification, which might result from the instability of M1. High resolution mass spectrum of M1 demonstrated its protonated molecule ion of *m*/*z* 287.0549 (Table 1), which agrees with the molecular weight of monohydroxylation of AE. The assignment of M2 as 5-hydroxy aloe-emodin enables us to propose that M1 was 7-hydroxy aloe-emodin, since hydroxyl substitutes

with electron donation property are well known to activate *ortho*- and *para*-carbons for electrophilic aromatic substitution.

Four GSH conjugates (M3-M6) were observed in NADPH- and GSH-fortified rat and human liver microsomes. M3 and M4 were found in the reaction system without NADPH (Figure 3A), demonstrating that P450 enzymes did not participate in the generation of M3 and M4. We anticipate that M3 and M4 were generated from direct reaction of AE with GSH. To verify the speculation, we allowed AE to react GSH in a buffer system. As expected, two products derived from GSH showed identical retention time and mass spectral identity (Figure 3C, F and G) as those of M3 and M4 found in microsomal reactions. M3 and M4 are most likely positional isomers resulting from adduction of GSH on different carbons of the aromatic ring of AE. Together, the results indicate that AE reacted with nucleophilic GSH without the assistance of enzyme catalysis. This enables us to speculate that AE can form protein covalent binding via the direct reaction of AE with cysteine residues of protein. The $[M]^+$ of M5 and M6 (*m*/*z* 592) were 16 Da higher than that of M3 and M4 (*m*/*z* 576), suggesting that M5 and M6 resulted from oxidative metabolites of AE. This encouraged us to define the metabolic routes of the two GSH conjugates by mixing of GSH with M1 or M2. We found that M5 originated from M1, and M6 came from M2 (Figures 4 C, E and 5 C, E).

Additionally, AE metabolism study was carried out in primary rat hepatocytes. Six metabolites, including M1−M6 as observed in microsomal incubations, were detected in primary rat hepatocytes treated with AE. GSH conjugates resulting from

direct adduction of AE or its hydroxylation metabolites with GSH were detected in AE-exposed cells, further providing the evidence for the reactivity of AE and oxidative metabolites of AE toward sulfhydryl-containing nucleophiles. The GSH conjugates observed in microsomal incubation and cultured primary hepatic cell exposure studies imply that AE and AE hydroxylation metabolites covalently bind to cysteine residues of proteins or other thiol-containing biomolecules, which could initiate the toxicities of AE and AE oxidative metabolites.

Two AE GSH conjugates (M3 and M4) and one hydroxylated AE GSH conjugate (M6) were observed in bile samples of animals treated with AE as detected in rat liver microsomal reactions. Unexpectedly, M5 was not detected in the bile. Inconsistence of *in vitro* vs *in vivo* data often takes place in drug metabolism studies, particularly that in microsomal vs animal studies. Microsomes contain limited drug metabolizing enzymes compared with that of animal models. In the present study, the microsomal incubations were set for P450-mediated oxidation reactions. GSH conjugates M3-M6 could further be metabolized by enzymes which were either not included in microsomes or were unable to work under the particular condition. This may explain the disagreement observed in the *in vitro* vs *in vivo* studies. GSH conjugates excreted in bile are generally employed as biomarkers of exposure to electrophilic agents.[24, 25] The observed GSH conjugates indicate that AE and its hydroxylation metabolite are all electrophilic species that have chemical reactivity toward the sulfhydryl of GSH to generate the corresponding GSH conjugates. It is most likely that these electrophiles alkylate cysteine-based protein. Protein covalent

binding has been considered as one of biochemical mechanisms by which various drugs and chemicals induce toxicities.[26, 27] This made us propose that modification of protein critical for cell maintenance may trigger the development of the cytotoxicity of AE. However, profound research needs to be done to verify the hypothesis. In addition, GSH conjugates are commonly metabolized to mercapturic acids which are then excreted in urine. It is reasonable to find NAC conjugate M7 in urine samples of rats given AE.

Given together, we propose the oxidative metabolism and GSH conjugation pathways of AE as shown in Scheme 1. The 1, 4-quinone moiety makes the parent compound reactive to thiols. AE directly reacts with GSH through Michael addition to generate GSH conjugate **1**. The conjugate is sequentially oxidized to M3/M4 via auto-oxidation. Additionally, AE undergoes P450-mediated hydroxylation to form M1 and M2, followed by GSH conjugation. The resulting GSH conjugates (**2** and **3**) are further oxidized to M5 and M6 as for the formation of M3/M4.

In conclusion, metabolic oxidation of AE produced two phase I metabolites, including 5-hydroxy aloe-emodin and possibly 7-hydroxy aloe-emodin. P450s 1A2, 3A4 and 3A5 participated in the observed AE hydroxylation. Both AE itself and hydroxylation metabolites are electrophilic species that have chemical reactivity to GSH. The findings certainly assist the understanding of the mechanisms of AE-induced cytotoxicity.

FUNDING SOURCES

This work was partly supported by the National Natural Science Foundation of China [Grant 81430086, 81773813, and 81830104].

SUPPORTING INFORMATION

LC-MS/MS analysis of M1-M6 in rat liver microsomal incubations; Tandem spectra of M1-M6 produced in rat microsomal reactions; ^{1}H NMR spectrum of M2.

ABBREVIATIONS

CE, collision energy; DMSO, dimethyl sulfoxide; DP, declustering potential; EPI, enhanced product ion; GSH, glutathione; IDA, information-dependent acquisition; LC-MS/MS, liquid chromatography-tandem mass spectrometry; MRM, multiple-reaction monitoring; NAC, *N*-acetylcysteine; NADPH, β -nicotinamide adenine dinucleotide 2'-phosphate reduced tetrasodium salt; FBS, fetal calf serum; DMEM, dulbecco's modified eagle's medium; HLMs, human liver microsomes; RLMs, rat liver microsomes; NMR, nuclear magnetic resonance.

REFERENCES

(1) Hu, B. Y., Zhang, H., Meng, X. L., Wang, F., and Wang, P. (2014) Aloe-emodin fromrhubarb (Rheum rhabarbarum) inhibits lipopolysaccharide-induced inflammatory responses in RAW264.7 macrophages. *J Ethnopharmacol*. *153*, 846-853.

(2) Ma, B. L., Ma, Y. M., Yan, D. M., Zhou, H., Shi, R., Wang, T. M., Yang, Y., Wang, C. H., and Zhang, N. (2009) Effective constituents in Xiexin Decoction for anti-inflammation. *J Ethnopharmacol*. *125*, 153-156.

(3) Öztürk, M., Aydoğmuş-Öztürk, F., Duru, ME., and Topçu, G. (2007) Antioxidant activity of stem and root extracts of Rhubarb (Rheum ribes): An edible medicinal plant. *Food Chem*. *103*, 623-630.

(4) Huang, Q., Lu, G., Shen, H. M., Chung, M. C., and Ong, C. N. (2007) Anti-Cancer Properties of Anthraquinones from Rhubarb. *Med Res Rev*. *27*, 609-630.

(5) He, Z. H., He, M. F., Ma, S. C., and But, P. P. (2009) Anti-angiogenic effects of rhubarb and its anthraquinone derivatives. *J Ethnopharmacol*. *121*, 313-317.

(6) Fang, X. L., Fang, Q., Luo, J. J., and Zheng, X. (2007) Effects of Crude Rhubarb on Intestinal Permeability in Septic Patients. *Am. J. Chin. Med*. *35*, 929-936.

(7) Xiao, B., Guo, J., Liu, D., and Zhang, S. (2007) Aloe-emodin induces in vitro G2/M arrest and alkaline phosphatase activation in human oral cancer KB cells. *Oral Oncol*. *43*, 905- 910.

(8) Li, M., Du, Z. M. (2015) Research progress on pharmacological effects of aloe-emodin. *Chin. J. Clin. Pharmacol*. *9*, 765-768.

(9) Chen, R. E., Zhang, J. M., Hu, Y. Y., Wang, S. P., Chen, M. W., and Wang, Y. T. (2014) Potential Antineoplastic Effects of Aloe-emodin: A Comprehensive Review. *Am. J. Chin. Med*. *42*, 275.

(10) Tseng, H. S., Wang, Y. F., Tzeng, Y. M., Chen, D. R., Liao, Y. F., Chiu, H. Y., and Hsieh, W. T. (2017) Aloe-Emodin Enhances Tamoxifen Cytotoxicity

by Suppressing Ras/ERK and PI3K/mTOR in Breast Cancer Cells. *Am. J. Chin. Med*. *45*, 337-350.

(11) Fenig, E., Nordenberg, J., Beery, E., Sulkes, J., and Wasserman, L. (2004) Combined effect of aloe-emodin and chemotherapeutic agents on the proliferation of an adherent variant cell line of Merkel cell carcinoma. *Oncol Rep*. *11*, 213-217.

(12) Thimmegowda, N. R., Park, C., Shwetha, B., Sakchaisri. K., Liu, K., Hwang, J., Lee, S., Jeong, S. J., Soung, N. K., Jang, J. H., Ryoo, I., Ahn. J. S., Erikson, R. L., and Kim, Bo. Y. (2015) Synthesis and Antitumor Activity of Natural Compound Aloe Emodin Derivatives. *Chem Biol Drug Des*. *85*, 638-644.

(13) Lee, H. Z., Lin, C. J., Yang, W. H., Leung, W. C., and Chang, S. P. (2006) Aloe-emodin induced DNA damage through generation of reactive oxygen species in human lung carcinoma cells. *Cancer Lett*. *239*, 55-63.

(14) Han, Z., Wei, W., Dunaway, S., Darnowski, J. W., Calabresi, P., Sedivy, J., Hendrickson, E. A., Balan, K. V., Pantazis, P., and Wyche, J. H. (2002) Role of p21 in Apoptosis and Senescence of Human Colon Cancer Cells Treated with Camptothecin. *J Biol Chem*. *277*, 17154-17160.

(15) Al-Otaibi, J. S., Spittle, P. T., and Gogary, T. M. E. (2017) Interaction of anthraquinone anti-cancer drugs with DNA: Experimental and computational quantum chemical study. *J Mol Struct*. *1127*, 751-760.

(16) Elgogary, T. M., and Elgendy, EM. (2003) Noncovalent attachment of psoralen derivatives with DNA: Hartree/Fock and density functional studies on the probes. *Spectrochim Acta A*. *59*, 2635-2644.

(17) Nesslany, F., Simarmeintières, S., Ficheux, H., and Marzin, D. (2009) Aloe-emodin-induced DNA fragmentation in the mouse in vivo comet assay. *Mutat Res-Gen Tox En*. *678*, 13-19.

(18) Vath, P., Wamer, W. G., and Falvey, D. E. (2002) Photochemistry and Phototoxicity of Aloe Emodin. *Photochem Photobiol*. *75*, 346-352.

(19) Strickland, F. M., Muller, H. K., Clifton Stephens, L., Bucana, C. D., Donawho, C. K., Sun, Y., Pelley, R. P. (2000) Induction of primary cutaneous melanoma in C3H mice by combined treatment with ultraviolet radiation, ethanol,

and aloe emodin. *Photochem. Photobiol*, *72*,407–414.

(20) Lin, D. J., Li, C. Y., Peng, Y., Gao, H. Y., and Zheng, J. (2014) Cytochrome P450-Mediated Metabolic Activation of Diosbulbin B. *Drug Metab Dispos*. *42*, 1727-1736.

(21) Seglen, P. O. (1976) Preparation of isolated rat liver cells. *Methods Cell Biol. 13*, 29-83.

(22) Banks, H. J., Cameron, D. W., and Raverty, W. D. (1978) Hydroxylation of Anthraquinones in Oleum and in Sulfuric Acid. *Aust. J. Chem*. *31*. 2271-82.

(23) Rodrigues, A. D. (1999) Integrated cytochrome P450 reaction phenotyping: attempting to bridge the gap between cDNA-expressed cytochromes P450 and native human liver microsomes. *Biochem Pharmacol*. *17*, 465-480.

(24) Yao, H. N., Peng, Y., and Zheng, J. (2016) Identification of glutathione and related cysteine conjugates derived from reactive metabolites of methyleugenol in rats. *Chemico-Biological Interactions. 253,* 143-152.

(25) Gopaul, S. V., Farrell, K., and Abbott, F. S. (2000) Identification and characterization of Nacetylcysteineconjugates of valproic acid in humans and animals. *Drug Metab. Dispos. 28,* 823-832.

(26) Hinson, D. H., and Roberts, D. W. (1992) Role of covalent and noncovalent interactions in cell toxicity: effects on proteins. *Annu. Rev. Pharmacol. Toxicol. 32,* 471-450.

(27) Boelsterli, U. A. (1993) Specific targets of covalent drug-protein interactions in hepatocytes and their toxicological significance in druginduced liver injury. *Drug Metab. Rev. 25,* 395-451.

Table 1. Mass spectrometric data acquired from high resolution mass spectrometric analysis of synthetic M1.

Figure Legends

Figure 1. Tandem mass spectrum of AE.

Figure 2. Characterization of M1 and M2. Ion chromatograms (*m*/*z* 287→241) gained from LC-MS/MS analysis of AE-fortified human liver microsomal reactions in the absence (A) or presence (B) of NADPH. Ion chromatograms (*m*/*z* 287→241) gained from LC-MS/MS analysis of synthetic M1 (C) and M2 (D). Tandem mass spectra of M1 (E) and M2 (F) produced in human liver microsomal reactions. Tandem mass spectra of synthetic M1 (G) and M2 (H).

Figure 3. Characterization of M3 and M4. Ion chromatograms (M3, *m*/*z* 576→301; M4, *m*/*z* 576→327) gained from LC-MS/MS analysis of AE-fortified human liver microsomal reactions supplemented with GSH in the absence (A) or presence (B) of NADPH. C: Ion chromatogram (*m*/*z* 576→301/327) gained from LC-MS/MS analysis of synthetic M3 and M4. D: Tandem spectrum of M3 generated in microsomal reactions. E: Tandem mass spectrum of M4 generated in microsomal reactions. F: Tandem mass spectrum of synthetic M3. G: Tandem mass spectrum of synthetic M4.

Figure 4. Characterization of M5. Ion chromatogram (*m*/*z* 592→317) gained from LC-MS/MS analysis of AE-fortified human liver microsomal reactions supplemented

with GSH in the absence (A) or presence (B) of NADPH. (C) Ion chromatogram (*m*/*z* 592→317) gained from LC-MS/MS analysis of synthetic M5. D: Tandem mass spectrum of M5 formed in human liver microsomal reactions. E: Tandem mass spectrum of synthetic M5.

Figure 5. Characterization of M6. Ion chromatograms (*m*/*z* 592→317) gained from LC-MS/MS analysis of AE-fortified human liver microsomal reactions trapped with GSH in the absence (A) or presence (B) of NADPH. C: Ion chromatogram (*m*/*z* 592 →317) gained from LC-MS/MS analysis of synthetic M6. D: Tandem spectrum of M6 formed in microsomal reactions. E: Tandem mass spectrum of synthetic M6.

Figure 6. Phase I metabolism of AE in rat hepatocytes. Ion chromatograms (*m*/*z* 287 →241) gained from LC-MS/MS analysis of rat hepatocytes before (A) and after (B) exposure to AE. Tandem mass spectra of M1 (C) and M2 (D) in hepatocytes treated with AE.

Figure 7. Phase II metabolism of AE in rat hepatocytes. Ion chromatograms (*m*/*z* 576 →301) gained from LC-MS/MS analysis of samples of rat hepatocytes before (A) and after (B) exposure to AE. Tandem mass spectra of M3 (C) and M4 (D) gained from analysis of samples prepared from hepatocytes after exposed to AE.

Figure 8. Phase I metabolism-involved phase II metabolism of AE in rat hepatocytes. Ion chromatograms (*m*/*z* 592 → 317) gained from LC-MA/MS analysis of rat hepatocytes before (A) and after (B) exposed to AE. Tandem mass spectra of M5 (C)

and M6 (D) in hepatocytes treated with AE.

Figure 9. Phase II metabolites of AE in bile. Ion chromatograms (*m*/*z* 576→301) gained from LC-MS/MS analysis of bile samples of animals before (A) or after (C) given AE. Tandem mass spectra of M3 (E) and M4 (F) in bile samples of animals administered AE. Ion chromatograms (*m*/*z* 592→317) gained from LC-MS/MS analysis of bile samples obtained from animals before (B) or after (D) given AE. G: Tandem mass spectrum of M6 in bile samples obtained from rats given AE.

Figure 10. Phase I metabolites of AE in urine. Ion chromatograms (*m*/*z* 287→241) gained from LC-MS/MS analysis of urine samples collected from rats before (A) or after (B, C) given AE. Tandem mass spectra of M1 (D) and M2 (E) of urine of animals administered AE.

Figure 11. AE-derived NAC conjugates *in vitro* and *in vivo*. Ion chromatograms (M7, *m*/*z* 448→317) gained from LC-MS/MS analysis of AE and NAC-supplemented rat liver microsomal incubations in the absence (C) of NADPH. Ion chromatograms of M7 gained from LC-MS/MS analysis of urine samples obtained from animals before (A) or after (B) given AE. E: Tandem mass spectrum of M7 generated in microsomal reactions. D: Tandem mass spectrum of M7 in the urine samples of rats given AE.

Figure 12. P450 enzymes responsible for AE hydroxylation. NADPH-fortified human recombinant P450 enzymes was individually incubated with AE in the absence

(A) or presence (B) of GSH. Data represent the mean ± SD (n= 3).

Scheme Legends

Scheme 1. Proposed cytochromes P450-mediated routes for the generation of AE metabolites.

Table 1.

compound	formula	$[M + H]^+$		error		sigma
		calulated	detected	ppm	mDa	
M1	$C_{15}H_{10}O_6$	287.0550	287.0549	0.16	0.6	19.7

Figure 1.

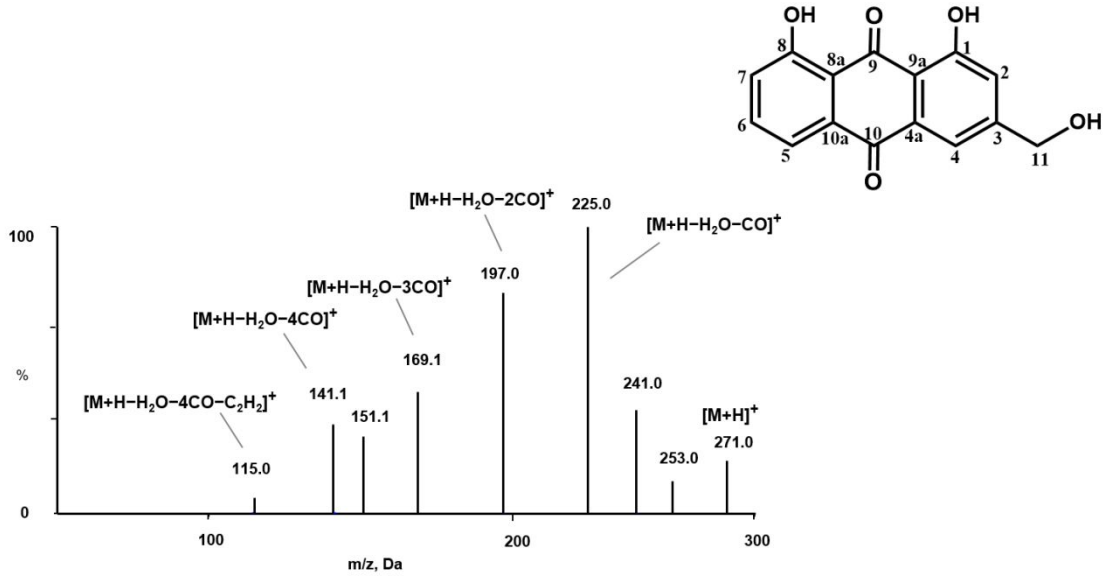
OH
O
OH
8
8a
9
9a
1
2
7
6
10a
10
4a
3
OH
5
4
11
O
100
%
0
[M+H−H2O−2CO]+
225.0
[M+H−H2O−CO]+
197.0
[M+H−H2O−3CO]+
[M+H−H2O−4CO]+
169.1
241.0
[M+H−H2O−4CO−C2H2]+
141.1
151.1
[M+H]+
271.0
253.0
115.0
100
200
300
m/z, Da

Figure 2.

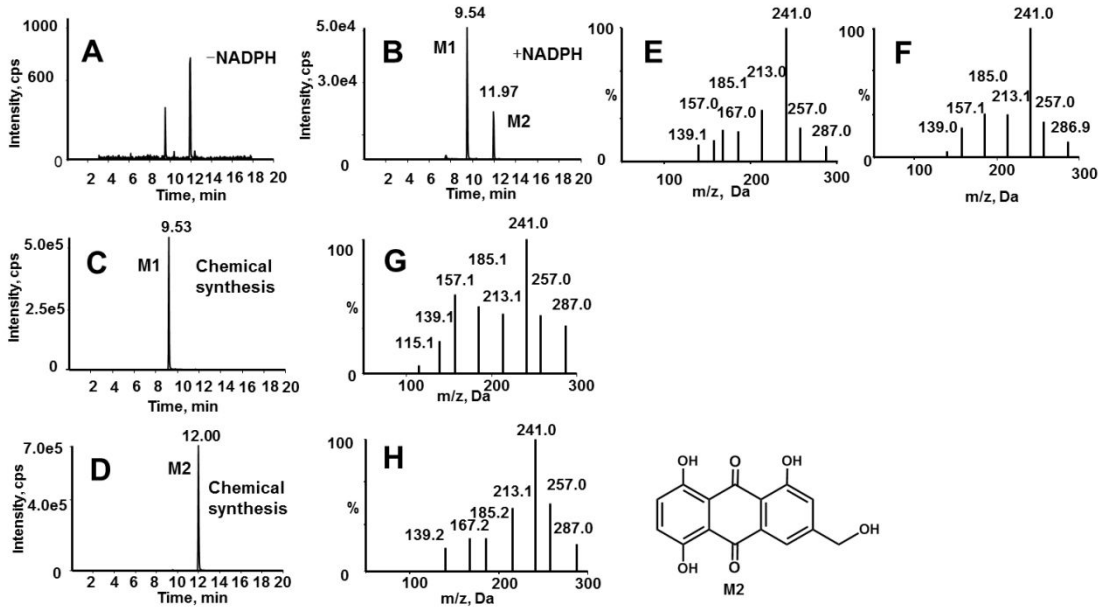
A
−NADPH
Intensity, cps
Time, min
B
M1
+NADPH
9.54
11.97
M2
E
241.0
213.0
185.1
157.0
167.0
257.0
139.1
287.0
m/z, Da
F
241.0
185.0
157.1
213.1
257.0
139.0
286.9
C
M1
Chemical synthesis
9.53
G
241.0
185.1
157.1
257.0
213.1
139.1
287.0
115.1
D
M2
Chemical synthesis
12.00
H
241.0
213.1
257.0
185.2
139.2
167.2
287.0
OH
M2

Figure 3.

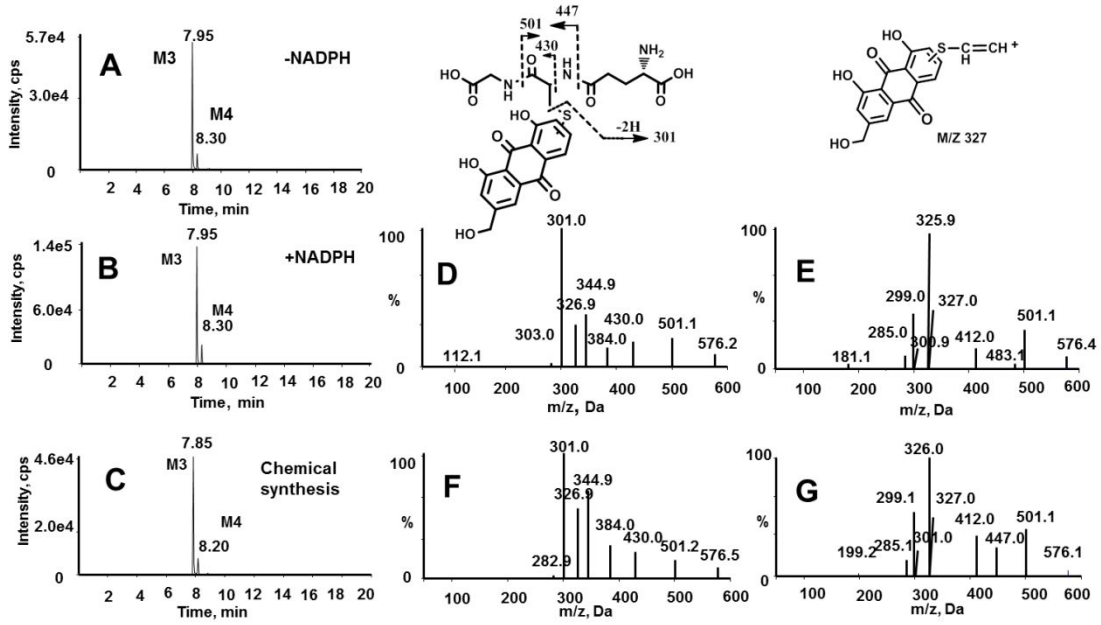
A
M3
-NADPH
M4
8.30
7.95
Intensity, cps
Time, min
B
+NADPH
C
Chemical synthesis
8.20
7.85
D
E
F
G
m/z, Da
501
447
430
-2H
301
M/Z 327
325.9
301.0
344.9
326.9
430.0
501.1
576.2
303.0
384.0
112.1
299.0
327.0
285.0
412.0
483.1
181.1
576.4
282.9
501.2
576.5
326.0
199.2
285.1
447.0
576.1

Figure 4.

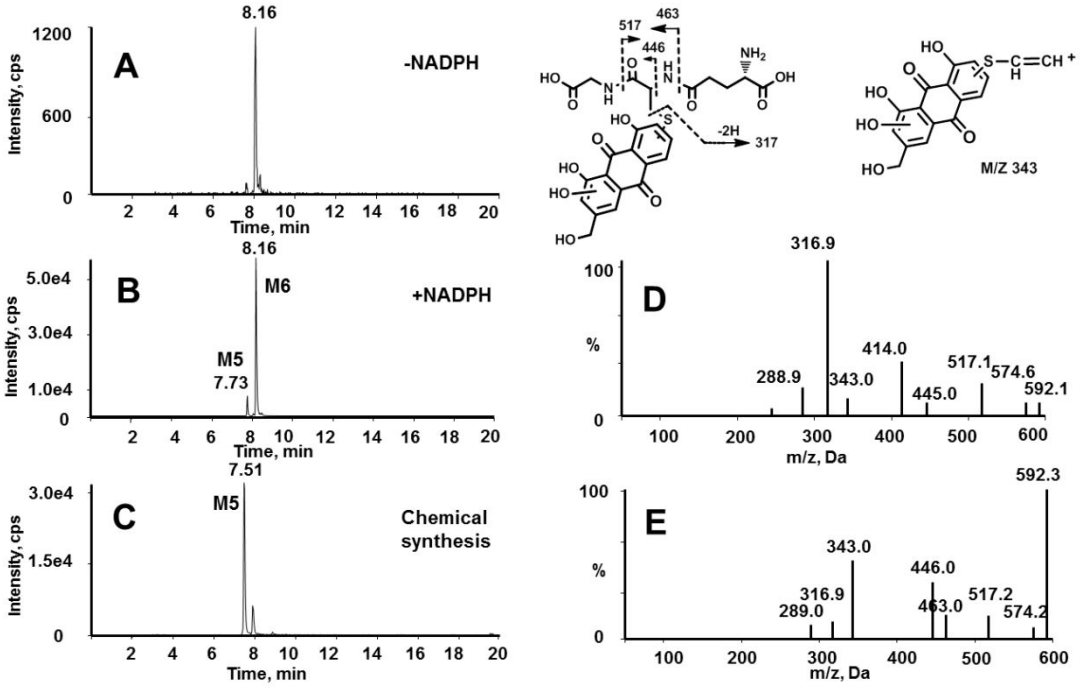
A
-NADPH
8.16
Intensity, cps
Time, min
B
+NADPH
M6
M5
7.73
C
Chemical synthesis
7.51
463
517
446
-2H
317
M/Z 343
D
316.9
414.0
517.1
574.6
592.1
288.9
343.0
445.0
m/z, Da
E
592.3
343.0
446.0
316.9
289.0
463.0
517.2
574.2

Figure 5.

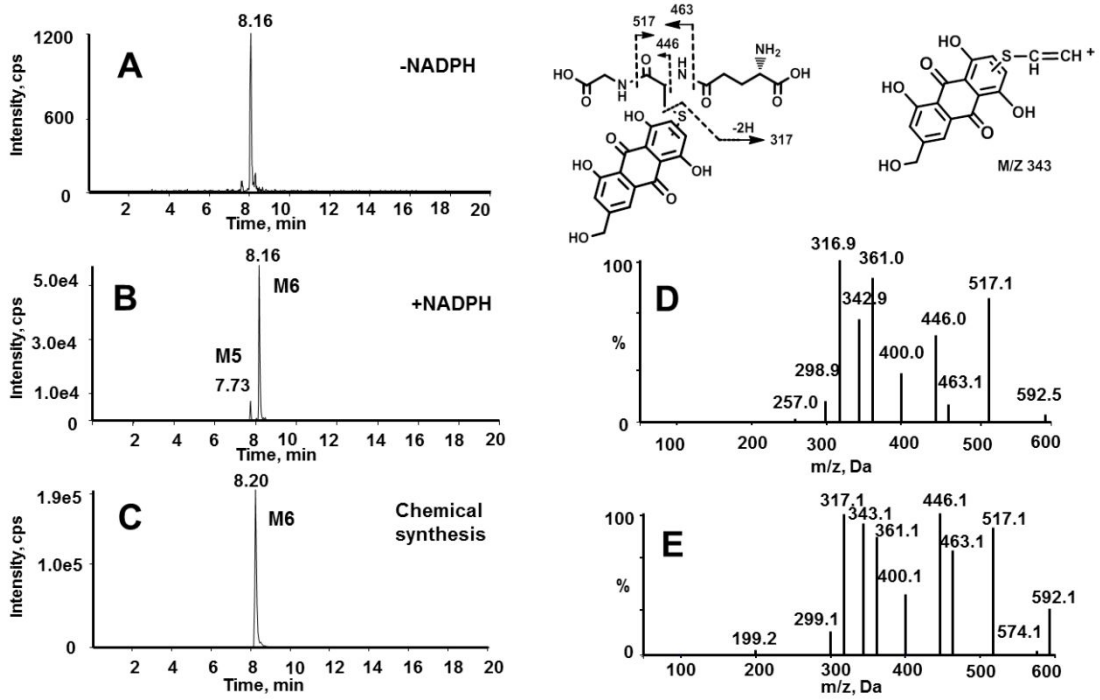
A
-NADPH
8.16
Intensity, cps
Time, min
B
+NADPH
M6
M5
7.73
C
Chemical synthesis
8.20
517
463
446
317
-2H
M/Z 343
D
316.9
361.0
342.9
517.1
446.0
400.0
298.9
463.1
257.0
592.5
m/z, Da
E
317.1
343.1
361.1
446.1
463.1
517.1
400.1
299.1
199.2
574.1
592.1

Figure 6.

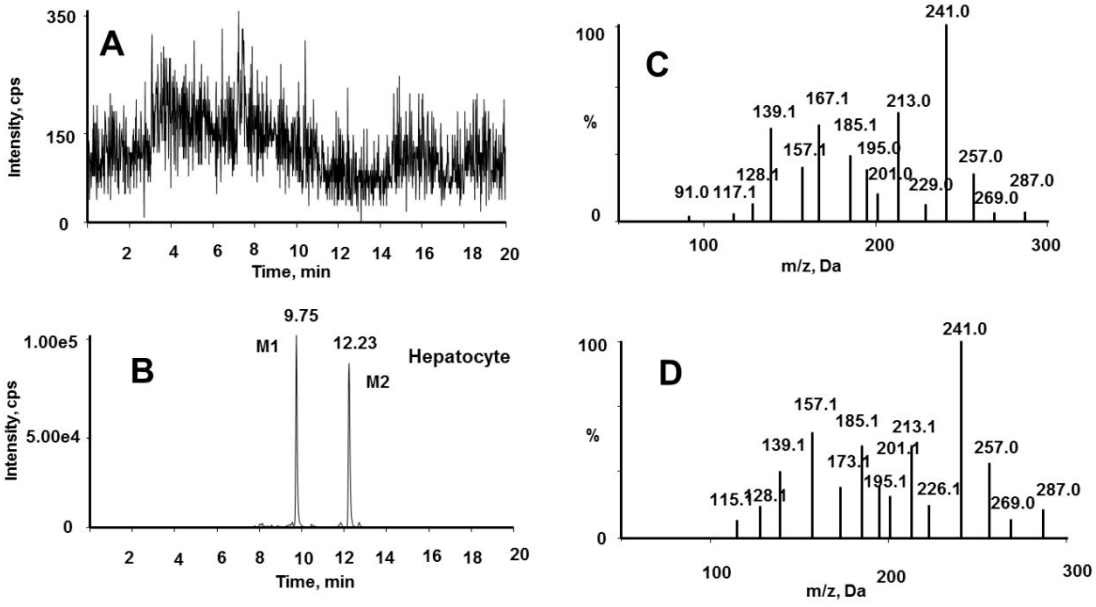
A
Intensity, cps
350
150
0
2 4 6 8 10 12 14 16 18 20
Time, min
B
Intensity, cps
1.00e5
5.00e4
0
9.75
M1
12.23
M2
Hepatocyte
2 4 6 8 10 12 14 16 18 20
Time, min
C
100
%
0
241.0
167.1
213.0
139.1
185.1
157.1
195.0
257.0
128.1
201.0
287.0
91.0 117.1
229.0
269.0
100 200 300
m/z, Da
D
100
%
0
241.0
157.1
185.1
213.1
139.1
201.1
257.0
173.1
195.1
226.1
115.1 128.1
269.0
287.0
100 200 300
m/z, Da

Figure 7.

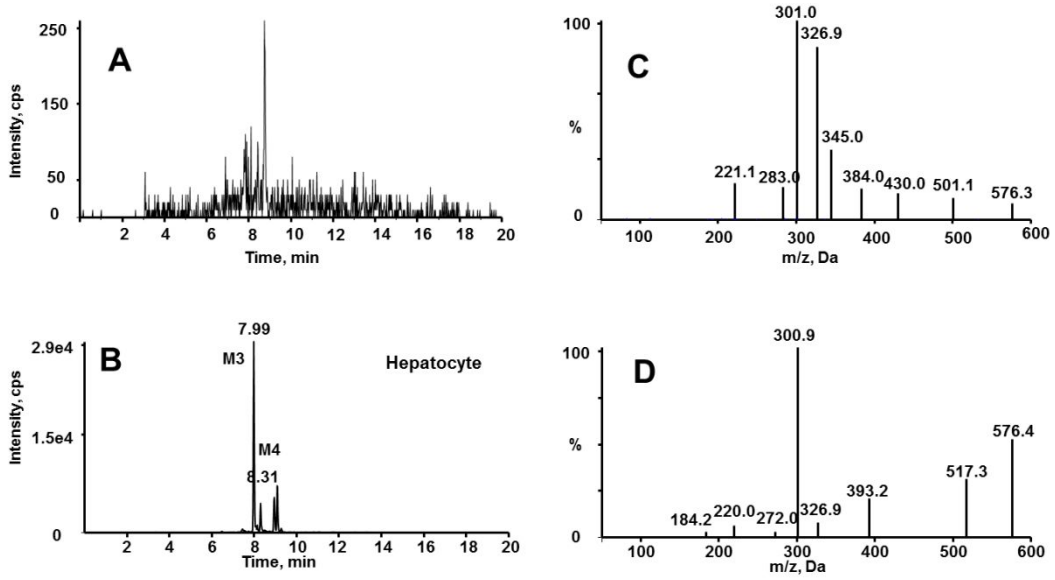
A
Intensity, cps
Time, min
B
M3
M4
7.99
8.31
Hepatocyte
C
301.0
326.9
345.0
221.1
283.0
384.0
430.0
501.1
576.3
m/z, Da
D
300.9
576.4
517.3
393.2
184.2
220.0
272.0
326.9

Figure 8.

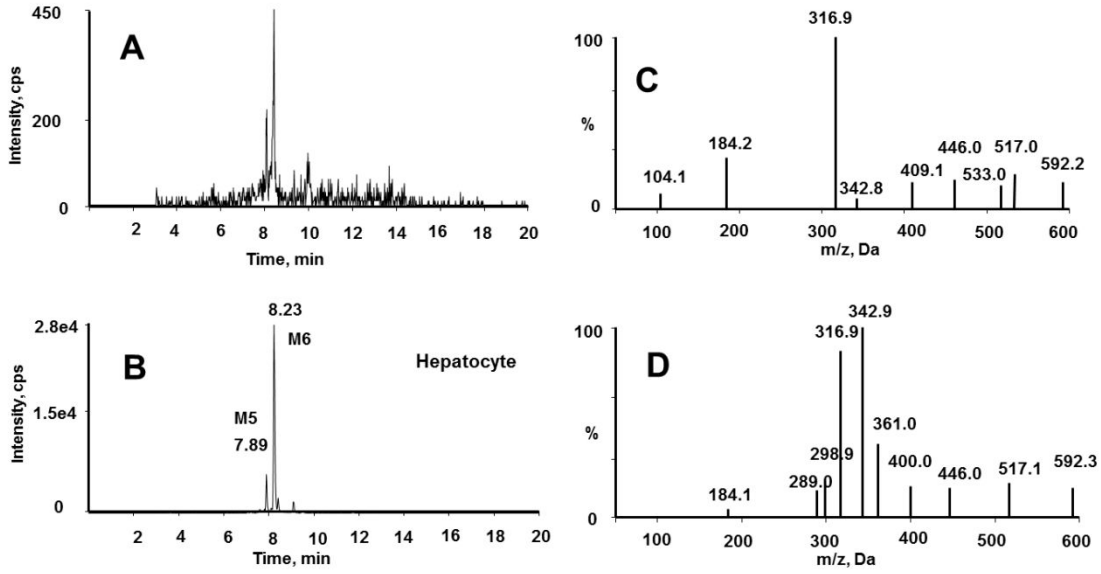
A
Intensity, cps
Time, min
B
Hepatocyte
M5
7.89
8.23
M6
C
316.9
184.2
104.1
342.8
409.1
446.0
533.0
517.0
592.2
m/z, Da
D
342.9
316.9
361.0
298.9
289.0
184.1
400.0
446.0
517.1
592.3
m/z, Da

Figure 9.

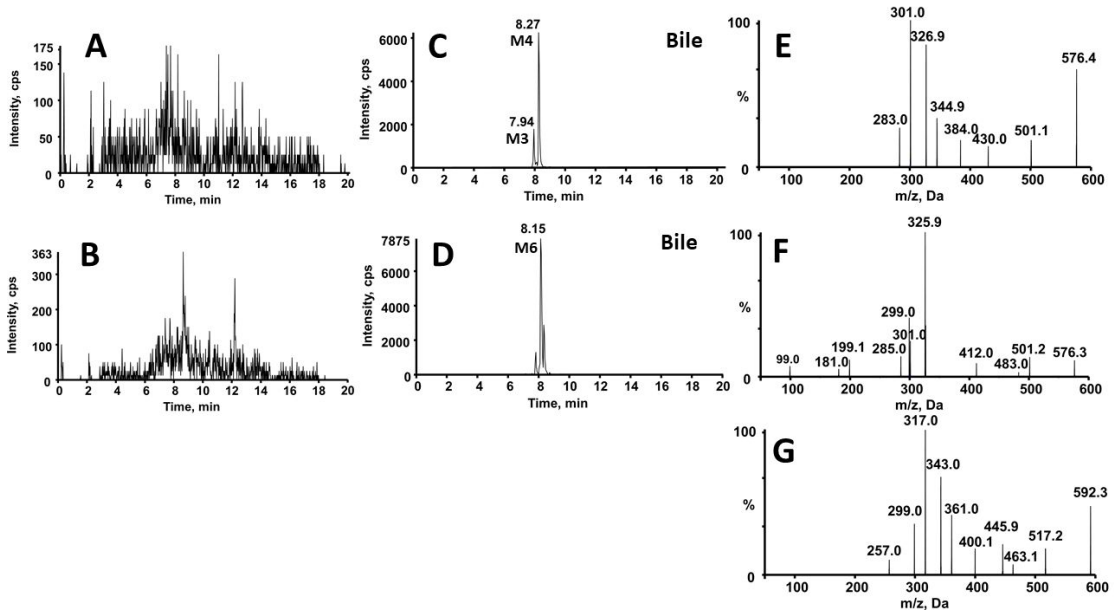
A
B
C
D
E
F
G
Bile
Bile
M4
M3
M6
8.27
7.94
8.15
Intensity, cps
Time, min
m/z, Da
%
301.0
326.9
576.4
344.9
283.0
384.0
430.0
501.1
325.9
299.0
301.0
199.1
285.0
181.0
99.0
412.0
501.2
483.0
576.3
317.0
343.0
592.3
299.0
361.0
445.9
400.1
517.2
257.0
463.1

Figure 10.

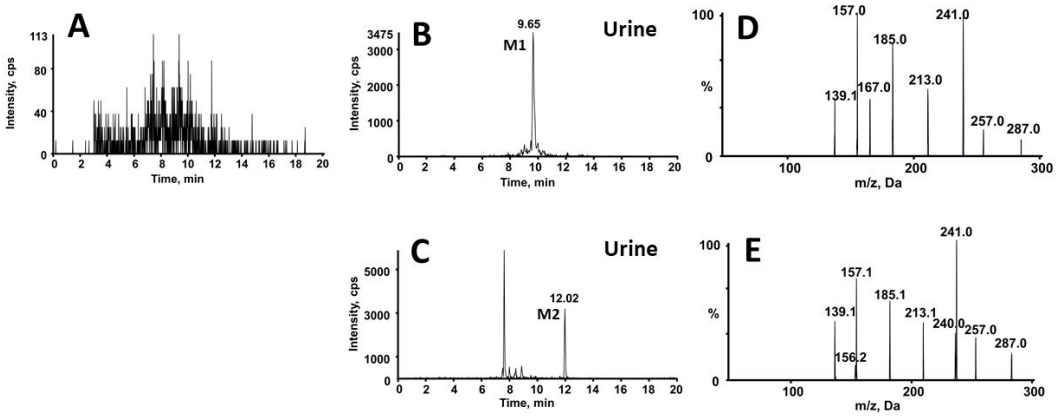
A
Intensity, cps
Time, min
B
Urine
M1
9.65
C
Urine
M2
12.02
D
157.0
241.0
185.0
213.0
139.1
167.0
257.0
287.0
m/z, Da
E
241.0
157.1
185.1
139.1
213.1
240.0
257.0
287.0
156.2
m/z, Da

Figure11.

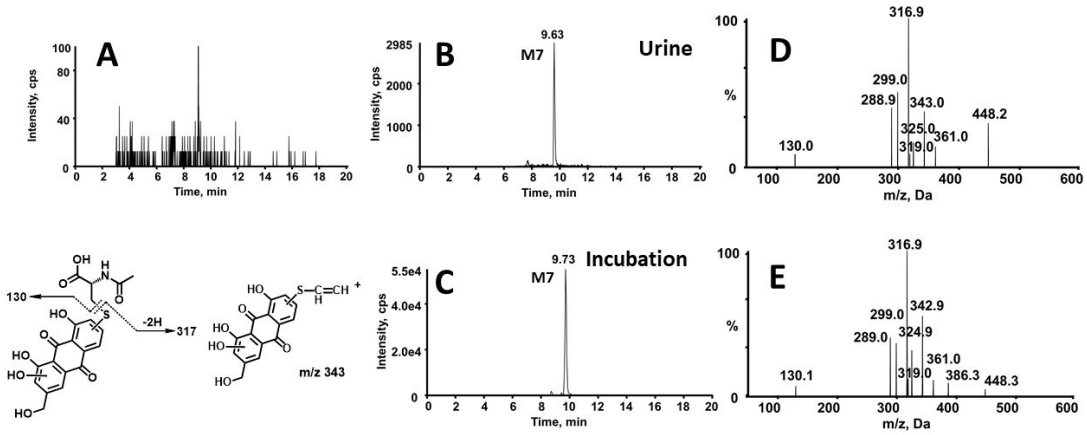
A
Intensity, cps
Time, min
B
M7
9.63
Urine
Intensity, cps
Time, min
D
316.9
299.0
288.9
343.0
448.2
325.0
361.0
319.0
130.0
%
m/z, Da
130
-2H
317
m/z 343
C
M7
9.73
Incubation
Intensity, cps
Time, min
E
316.9
342.9
299.0
324.9
289.0
361.0
319.0
386.3
448.3
130.1
%
m/z, Da

Figure 12.

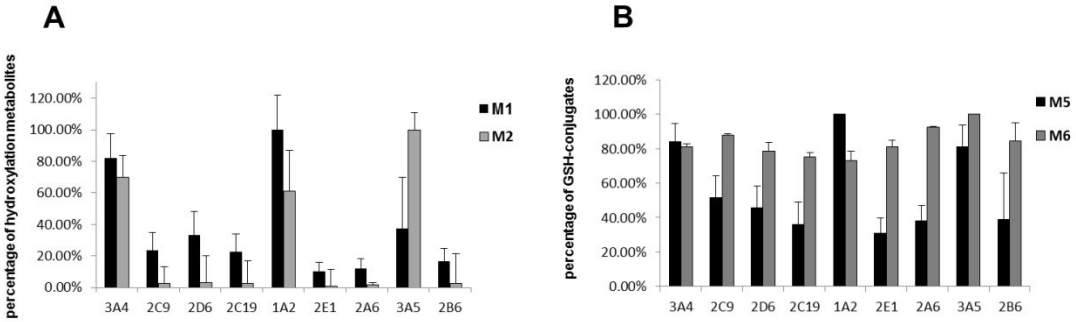
A
percentage of hydroxylation metabolites
120.00%
100.00%
80.00%
60.00%
40.00%
20.00%
0.00%
M1
M2
3A4 2C9 2D6 2C19 1A2 2E1 2A6 3A5 2B6
B
percentage of GSH-conjugates
120.00%
100.00%
80.00%
60.00%
40.00%
20.00%
0.00%
M5
M6
3A4 2C9 2D6 2C19 1A2 2E1 2A6 3A5 2B6

Scheme 1.